Calibration of a dual-laser triangulation system for assembly line completeness inspection

Conference Paper · November 2012

DOI: 10.1109/ROSE.2012.6402621

CITATIONS
10

READS
228

3 authors, including:

Stefano Michieletto
University of Padova
43 PUBLICATIONS **223** CITATIONS

SEE PROFILE

Emanuele Menegatti
University of Padova
225 PUBLICATIONS **2,158** CITATIONS

SEE PROFILE

Calibration of a Dual-Laser Triangulation System for Assembly Line Completeness Inspection

Edmond Wai Yan So, Stefano Michieletto, and Emanuele Menegatti
Intelligent Autonomous Systems Laboratory, Department of Information Engineering, University of Padua
Padua, Italy
{edmond.so, stefano.michieletto, emg}@dei.unipd.it

***Abstract*— In controlled industrial environments, laser triangulation is an effective technique for 3D reconstruction, which is increasingly being used for quality inspection and metrology. In this paper, we propose a method for calibrating a dual laser triangulation system – consisting of a camera, two line lasers, and a linear motion platform – designed to perform completeness inspection tasks on an assembly line. Calibration of such a system involves the recovery of two sets of parameters – the plane parameters of the two line lasers, and the translational direction of the linear motion platform. First, we address these two calibration problems separately. While many solutions have been given for the former problem, the latter problem has been largely ignored. Next, we highlight an issue specific to the use of multiple lasers – that small errors in the calibration parameters can lead to misalignment between the reconstructed point clouds of the different lasers. We present two different procedures that can eliminate such misalignments by imposing constraints between the two sets of calibration parameters. Our calibration method requires only the use of planar checkerboard patterns, which can be produced easily and inexpensively.**

Keywords- laser traingulation, laser calibration, conveyor calibration, dual lasers, misalignment

I. INTRODUCTION

A. Dual Laser Triangulation System

Machine vision is widely used for quality control tasks in industrial environments. Increasingly, 3D measurement technology in the form of structured light sensors and time-of-flight cameras is being used in such applications to provide depth information.

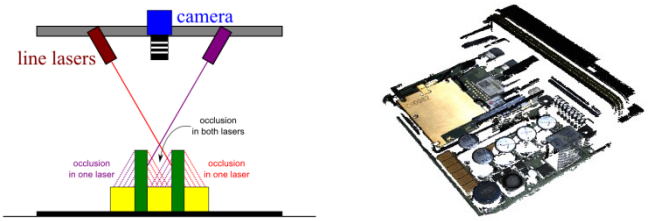

(a) (b)

Figure 1. (a) Sensors configruation in our Dual Laser Triangulation System. (b) Colored point cloud of a sample reconstructed by the our sytem.

Previously, we have presented the "*Dual Laser Triangulation System*" (DLTS) [1] [2] – consisting of a color CCD camera, two line lasers, and a line light (Fig. 1a) – as a demonstration of a low-cost color 3D model acquisition system built with commonly available machine vision components. By simultaneously capturing both laser range data and color texture data, the system produces a colored point cloud model (Fig. 1b) of scanned objects that can be used to perform completeness inspection tasks on assembly lines.

Compared with a single laser system, a dual laser configuration reduces the amount of occlusion, allowing objects with undulating surface geometries to be reconstructed more accurately. Additionally, by positioning the lasers and cameras appropriately, different range resolutions can be achieved by the two lasers, enabling the system to capture both the macroscopic geometry of the scanned object as well as microscopic surface details that may be important for defect inspection.

B. Overview of a Laser Triangulation System

In a laser triangulation system (Fig. 2), a line laser projects a plane of light onto the scene. The intersection of the plane of light with the surface of the scanned object results in a curve that is detected by a camera. If the parameters of the plane of light with respect to the camera's coordinate system is known, the 3D coordinates of the points on the imaged laser curve can be recovered. By either moving the scanned object (e.g., on a conveyor belt) or the sensor assembly (e.g. with a robot arm or a linear motion platform), a dense reconstruction of the surface of the scanned object can be created.

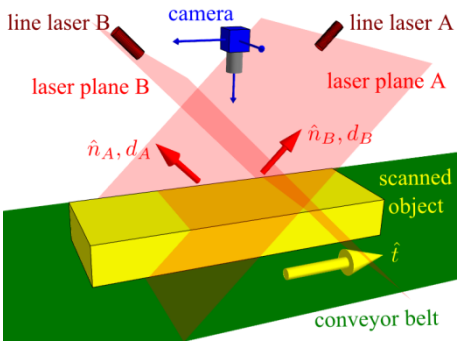

Figure 2. Basic setup of a laser triangulation system.

In order to perform the reconstruction, three sets of calibration parameters are required:

This research has received funding from IT+Robotics (http://www.it-robotics.it) and the European Union's Seventh Framework Programme for Research and Technological Development (http://ec.europa.eu/research/fp7/) under grant agreement No. 262009.

- camera intrinsic parameters (focal length, principal point, distortion coefficients)
- laser light plane parameters ($\hat{\boldsymbol{n}}_A, d_A, \hat{\boldsymbol{n}}_B, d_B$)
- direction of translational motion ($\hat{\boldsymbol{t}}$)

In the following, we will refer to the recovery of these sets of parameters respectively as camera calibration, laser calibration, and motion calibration.

C. Related Work

Many solutions have been given for calibrating a laser triangulation system. The underlying concept is to project the line laser onto a calibration rig with known world coordinates. In [3], Chen uses a calibration rig consisting of lines with known parameters. The intersection of the laser plane with each line gives an image point to world line correspondence. With six or more such correspondences, a 4x3 transformation matrix which maps a 2D image point to its 3D coordinate on the laser plane can be recovered. The linear transformation matrix encodes both the camera intrinsic parameters (excluding the distortion coefficients) as well as the laser plane parameters. In [4], Reid gives a similar solution, using a calibration rig consisting of planes with known parameters. Projecting the line laser onto the known planes gives an image point to world plane correspondence, and eight or more such correspondences are used to recover the 4x3 transformation matrix. In [5], Huynh uses a calibration rig consisting of two planes with 12 points with known 3D coordinates. The points form 4 straight lines, and by using the projective cross-ratio invariance, the 3D coordinates of the point of intersection of the laser plane with these 4 lines can be determined, giving image point to world point correspondences that are used to recover the 4x3 transformation matrix.

In [6], Trucco uses a sophisticated staircase calibration target to construct a lookup table, mapping 2D integer pixel coordinates to their 3D coordinates. In addition to the camera intrinsic parameters and the laser plane parameters encoded in the 4x3 transformation matrix above, the lookup table also account for the nonlinear effects of camera lens distortion. Although a lookup table allows for very fast triangulation, there is a slight decrease in accuracy because linear interpolation is used to transform sub-pixel image locations to their 3D coordinates.

The above calibration methods require a calibration rig with known world coordinates, established either by using some other measurement system, or by using a calibration object created with precise specifications. More flexible and economical solutions are given by Zhou [7] and Yamauchi [8], where only a planar calibration board placed at arbitrary orientations is required, similar to the popular solution by Zhang [9] for camera calibration. The camera is assumed to be already calibrated, thus its intrinsic parameters are known. An image of the calibration board is captured, along with the line of its intersection with the laser plane. Using correspondences between points on the calibration board and their imaged coordinates, the pose of the calibration board with respect to the camera center can be determined, resulting in a known world plane. The image of the laser line is then back-projected onto this known world plane, giving their 3D coordinates. Repeating this with the calibration board at different orientations result in a 3D point cloud spanning the laser plane, from which the laser plane parameters can be explicitly recovered.

All of the above focus either on a combined camera and laser calibration, or laser calibration alone. Motion calibration is not considered. In some cases, the system is mounted on a robot arm which is assumed to be calibrated, or on a mobile robot whose motion is estimated by other means. In other cases, the system considered is a structured-light system where multiple laser planes are being projected from a single source, so that motion is not required. In the remaining cases, the system considered does incorporate a linear motion platform, but the estimation of the direction of translational motion is simply not addressed as part of the calibration solution.

To our knowledge, only the solution given by McIvor [10] addresses motion calibration. In his solution, a 3D calibration object consisting of three planes approximately perpendicular to each other is used. The relative orientation between the planes are known, as are the locations of fiducial marks on these planes. The calibration object is moved on a linear motion platform, and the intersection of the laser plane with the fiducial marks is used to recover all three sets of calibration parameters explicitly.

D. Paper Outline

In this paper, we assume that the camera has been calibrated, and we focus on laser and motion calibration. First, we treat these two calibration problems separately. In §II, we give a solution for laser calibration that is similar to Zhou [7] and Yamauchi [8], using a planar calibration board placed at arbitrary orientations. However, we use a standard checkerboard calibration pattern that can be automatically detected using open source software. In §III, we present our solution for motion calibration. We consider three different situations for the linear motion platform: no encoder is used, so a constant velocity is assumed, as is the case considered by McIvor [10]; an encoder is present along with a known conversion factor; an encoder is present with unknown conversion factor which can be recovered as part of the calibration. Addressing all these different scenarios makes our calibration procedure applicable to a wide range of setups in industrial assembly line environments.

In §IV, we show that when multiple lasers are used, small errors in the calibration parameters can lead to misalignment between the reconstructed point clouds of the different lasers. In §V, we present two different procedures that can be used to eliminate this misalignment by imposing constraints between the two sets of calibration parameters. In §VI, we give some experimental results as validation of our solution. In §VII, we give concluding remarks and possible future improvements.

II. Laser Calibration

In this section, we explain how the parameters of the two laser planes in DLTS are recovered. As shown in Fig. 3, this involves placing a planar checkerboard pattern at arbitrary orientations in front of the sensor, so that both the checkerboard pattern and the intersection with both laser planes are imaged. This is similar to the solutions by Zhou [7] and

Yamauchi [8], but we use a standard checkerboard pattern that can be automatically detected using software.

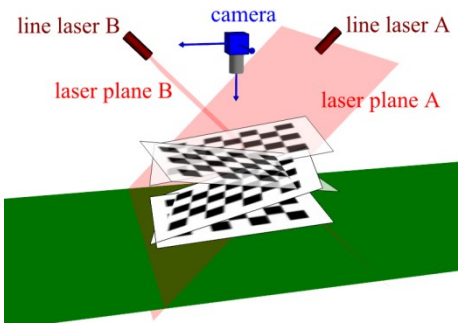

Figure 3. Laser calibration using planar checkerboards placed at arbitrary orientations.

A. Checkerboard Detection and Pose Estimation

The checkerboard pattern can be automatically detected using software such as the OpenCV library [11] or the GML C++ Camera Calibration Toolbox [12]. To ensure that the checkerboard pattern can be automatically detected even when two laser lines are present, we use the following strategies. First, the pattern is sized to cover only a small central area of the calibration board. We position the calibration board appropriately so that the laser lines not cut across the checkerboard pattern, but only through the bordering squares at the most (Fig. 4a-b). Second, because red (635nm wavelength) line lasers are used in our system, we use only the blue channel of the image for checkerboard detection, instead of the grayscale image converted from the RGB channels (Fig. 4c).

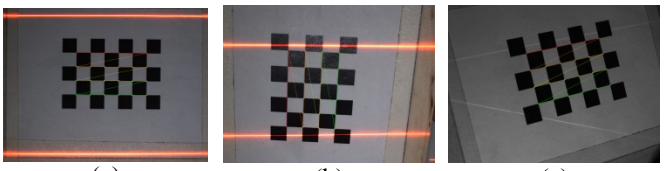

(a) (b) (c)

Figure 4. Automatic checkerboard detection. (a)-(b) The checkerboard pattern is sized sufficiently small so that the laser lines only cut across the bordering squares at the most. (d) Instead of using the grayscale image, only the blue channel is used for checkerboard detection.

Using correspondences between the checkerboard corners and their imaged coordinates, the pose of the calibration board with respect to the camera center can be determined. This is problem is known in computer vision as pose estimation, or the perspective N-point (PnP) problem [14]. The OpenCV library [11] and the Matlab Camera Calibration Toolbox [13] offers readily available functions to compute the optimal pose which minimizes the re-projection errors. For each checkerboard pose i, we can recover its plane parameters (plane normal $\hat{\boldsymbol{n}}_i$ and signed distance d_i from the camera center) from its pose parameters (rotation $\boldsymbol{R}_i$ and translation $\vec{\boldsymbol{t}}_i$) as:

$$\begin{aligned} \hat{\boldsymbol{n}}_i &= \boldsymbol{R}_i \cdot \begin{bmatrix} 0 \\ 0 \\ 1 \end{bmatrix} \\ d_i &= -\hat{\boldsymbol{n}}_i^T \vec{\boldsymbol{t}}_i \end{aligned} \tag{1}$$

B. Laser Points Detection and Triangulation

For each checkerboard pose, the calibration board is positioned carefully so that each laser line is always captured in either the top or bottom half of the image (i.e., in Fig. 3, the calibration board is positioned below the intersection of the two laser planes). For each half of an image, the position of the laser line is determined using the parabolic estimator [15] as follows. First, the intensities across the red, green, and blue channels are summed for each pixel. Then, across each column, the peak position of the summed intensity values is located. Finally, we determine the location of the laser line to sub-pixel accuracy by fitting a quadratic function to the summed intensities values in a window spanning 5 pixels surrounding the peak position (Fig. 5a).

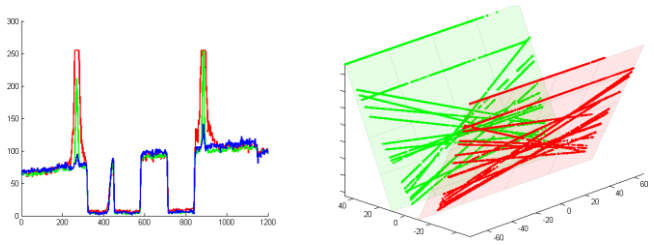

(a) (b)

Figure 5. (a) Intensity values across the RGB channels across an image column. (b) The triangulated laser points from mutliple checkerboard poses.

We recover the 3D coordinates of each laser point from its image coordinate $[u_j, v_j]$ as follows. First, given the camera calibration matrix K containing the focal length f and the principal point $[u_c, v_c]$, the normalized image coordinates of the laser point is $[x_j, y_j, 1]^T = K^{-1} \cdot [u_j, v_j, 1]^T$. The 3D coordinates $\boldsymbol{X}_j = [X_j, Y_j, Z_j]^T$ of the laser point is then the intersection of the ray from the camera center $\boldsymbol{O}_c = [0,0,0]^T$ through the normalized image point $\boldsymbol{x}_j = [x_j, y_j, 1]^T$, with the i^{th} calibration plane $\boldsymbol{\pi}_i = (\hat{\boldsymbol{n}}_i, d_i)$, i.e., a line-plane intersection problem:

$$\boldsymbol{X}_j = \frac{d_i}{\hat{\boldsymbol{n}}_i^T \boldsymbol{x}_j} \boldsymbol{x}_j \tag{2}$$

C. Recovering the Laser Planes Parameters

After repeating the above two steps with the calibration board at different orientations, we get two 3D point clouds $\boldsymbol{X}_A = \{\boldsymbol{X}_{jA}\}$, $\boldsymbol{X}_B = \{\boldsymbol{X}_{jB}\}$ spanning the laser planes $\boldsymbol{\pi}_A = (\hat{\boldsymbol{n}}_A, d_A)$ and $\boldsymbol{\pi}_B = (\hat{\boldsymbol{n}}_B, d_B)$. The laser plane parameters $(\hat{\boldsymbol{n}}_L, d_L)$, $L \in \{A, B\}$, are recovered by finding the best-fit plane to each of the point clouds.

The best-fit plane is defined as the one which minimizes the its orthogonal distance to each point in the point-cloud, $\sum(\boldsymbol{X_j} - \boldsymbol{X_0})^T \hat{\boldsymbol{n}}$, where $\boldsymbol{X_0}$ is a point on the plane. This can be solved in closed form using principal component analysis or SVD [16]. First, it can be shown that centroid of the point cloud, $\bar{\boldsymbol{X}} = \frac{1}{n}\sum \boldsymbol{X_j}$, lies on the best-fit plane. Then, expressing each point with respect to its point cloud centroid, $\tilde{\boldsymbol{X}}_j = \boldsymbol{X_j} - \bar{\boldsymbol{X}}$, we form a matrix $\boldsymbol{M} = [\tilde{\boldsymbol{X}}_1, \ldots, \tilde{\boldsymbol{X}}_j, \ldots]^T$. The problem is

then to find the plane normal $\hat{\boldsymbol{n}}_L$ which minimizes $\boldsymbol{M}^{\boldsymbol{T}}\hat{\boldsymbol{n}}_L$, subject to $\|\hat{\boldsymbol{n}}_L\| = 1$. Performing a singular value decomposition on the matrix $\boldsymbol{M} = \boldsymbol{USV}^{\boldsymbol{T}}$, the normal to the best fit plane is then the last column of the matrix $\boldsymbol{V}$.

$$\begin{aligned} \hat{\boldsymbol{n}}_L &= \boldsymbol{V} \cdot \begin{bmatrix} 0 \\ 0 \\ 1 \end{bmatrix} \\ d_L &= -\hat{\boldsymbol{n}}_L{}^T \bar{\boldsymbol{X}} \end{aligned} \tag{3}$$

III. Motion Calibration

In this section, we explain how to recover the direction of the translational motion a conveyor belt relative to the laser triangulation sensors. We consider three scenarios for the measurement of the translational motion:

- no encoder is used, so a constant velocity is assumed
- an encoder is present with a known conversion factor (e.g., mm/encoder count)
- an encoder is present with unknown conversion factor

A. Checkerboard Pattern

We use a calibration board containing three checkerboard patterns printed on the same piece of paper, as shown in Fig. 6. Each checkerboard pattern is wide and short, so that they cover a large part of an image in the horizontal direction, but a small part in the vertical direction, allowing the pattern to be captured at different positions along the translational path of the system.

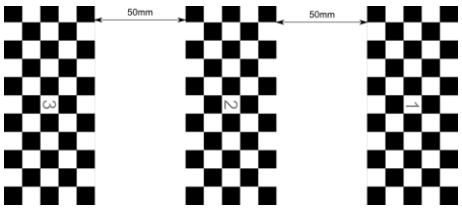

Figure 6. Checkerboard patterns used for motion calibration.

In our DLTS, the camera has a vertical FOV of 18.7°, and placed at a distance of 350mm from the conveyor belt, giving a vertical coverage of 115mm. Each checkerboard pattern measures 110x50mm, so the maximum translation possible is 65mm while keeping the pattern within the camera's field-of-view. By using three checkerboard patterns, the translational motion is increased by more than four times to 265mm. By increasing the magnitude of the translational motion, the estimation of the translational direction will be more robust against errors in the pose estimation of the calibration planes, stemming from noise in localization of the checkerboard corners.

Although the same effect can be achieved with coded markers, standard checkerboard patterns offers two advantages. First, open-source software for automatic detection is readily available. Second, a higher degree of accuracy can be achieved in the localization of corner features over circular features common in coded markers.

B. Constrained Pose Estimation

The calibration board is placed on the conveyor belt and translated under the camera (Fig. 7). Images of the checkerboard patterns are captured at various positions. For each image, the image coordinates of the checkerboard corners are automatically detected, and their corresponding world coordinates are generated based on the known separation between the patterns. Also, if an encoder is present, the difference in encoder counts ΔE_i from the first image is recorded; otherwise, the difference in time Δt_i from the first image is recorded instead.

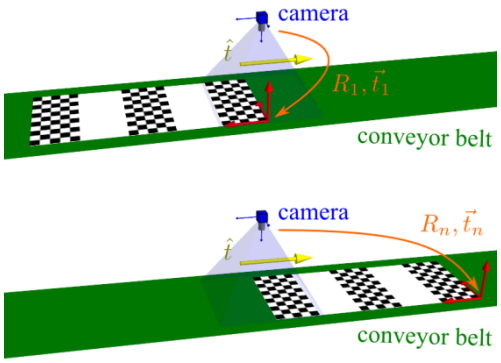

Figure 7. Motion calibration procedure.

For each imaged checkerboard pattern, the correspondences between the checkerboard corners $\boldsymbol{X}_j$ and their imaged coordinates $\boldsymbol{x}_j$ allows an independent estimate $(\boldsymbol{R}_i, \vec{\boldsymbol{t}}_i)$ of the pose of the calibration board. To recover the direction of translational motion, we formulate a single pose estimation problem involving all of image-to-world correspondences with the following two constraints:

- because the calibration board is undergoing pure translation, all of the poses have the same rotation, $\boldsymbol{R} = \boldsymbol{R_1} = \cdots = \boldsymbol{R_i}$
- the translation $\vec{\boldsymbol{t}}_{\boldsymbol{i}}$ from the camera to each checkerboard pose is offset from the first checkerboard pose $\vec{\boldsymbol{t}}_{\boldsymbol{1}}$ in the same direction $\hat{\boldsymbol{t}}$, $\vec{\boldsymbol{t}}_{\boldsymbol{i}} = \vec{\boldsymbol{t}}_{\boldsymbol{1}} + \mu_i \hat{\boldsymbol{t}}$.

Here μ_i is the magnitude of the translation motion, $\hat{\boldsymbol{t}}$ is the translational direction being seek in the current motion calibration.

The magnitude of the translation motion is determined as follows. If an encoder is not present, $\mu_i = v\Delta t_i$, where v is the speed of the linear motion platform; if v is unknown, it can be estimated as part of the constrained pose estimation problem. If an encoder is present, $\mu_i = \tau \Delta E_i$, where τ is the encoder conversion factor; if it is unknown, it can be estimated as part of the constrained pose estimation problem.

When the calibration board is placed parallel on the conveyor belt, $\hat{\boldsymbol{t}}$ must lie in the plane of the calibration board. Thus, it is parameterized using 1 DOF, $\hat{\boldsymbol{t}} = cos\theta \hat{\boldsymbol{\imath}} + sin\theta \hat{\boldsymbol{\jmath}}$, where $\hat{\boldsymbol{\imath}} = \boldsymbol{R} \cdot [1\ 0\ 0]^T$ and $\hat{\boldsymbol{\jmath}} = \boldsymbol{R} \cdot [0\ 1\ 0]^T$.

The constrained pose estimation problem is solved by minimizing the following by nonlinear least squares cost

function, which minimizes the reprojection errors of the imaged checkerboard corners:

$$\underset{\boldsymbol{R},\vec{\boldsymbol{t}}_1,\theta,[v|\tau]}{argmin} \sum_j \left\| \boldsymbol{x_j} - \boldsymbol{K} \cdot \left[\boldsymbol{R}|\vec{\boldsymbol{t}}_i\right] \cdot \boldsymbol{X_j} \right\|^2 \quad (4)$$

Instead of $6n$ DOF for n checkerboard poses, the constrained problem has 7 or 8 DOF, corresponding to 6DOF for the first checkerboard pose, 1DOF for $\hat{\boldsymbol{t}}$, and 1 DOF for v or τ if desired. An initial estimate can be obtained by performing an unconstrained pose estimation with the first and last checkerboard poses. The above cost function can then minimized using the Levenberg- Marquardt algorithm.

IV. Misalignment Between Point Clouds

Using the calibration procedures from §II and §III, we recover the laser and motion calibration parameters for our DLTS. However, as shown in Fig. 8, a reconstruction of the conveyor belt plane and a rectangular block reveals a significant offset between the point clouds of the two lasers. The offset in the vertical direction ranges from 3-5mm .

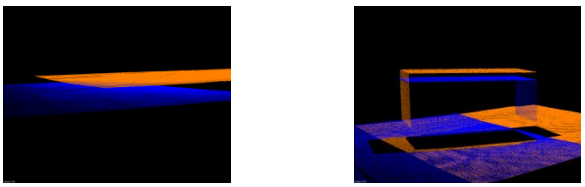

(a) (b)

Figure 8. Reconstructions showing offset between the point clouds of the two lasers. (a) Conveyor plane. (b) Rectangular block.

As shown by Fig. 9 for the 2D case, when two lasers are used in a triangulation system, errors in the either the laser plane parameters or the translational direction will lead to misalignment between the two point clouds in the reconstruction of a single plane. When laser calibration and motion calibration are performed separately, this misalignment cannot be detected from the calibration data.

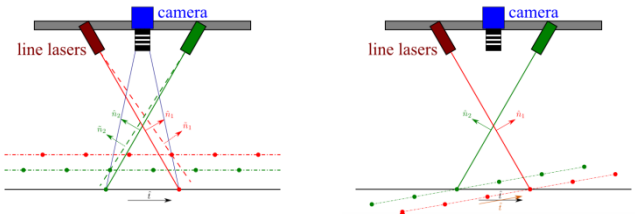

(a) (b)

Figure 9. (a) Rectangular block. (b) Reconstruction showing offset between the point clouds of the two lasers.

V. Constrained Calibration

In order to detect and correct the misalignment between the point clouds during calibration, a calibration procedure in which the calibration data is constrained by both the laser and motion parameters is required. We present two solutions; the first method uses the laser plane parameters to constrain the motion calibration, while the second method uses the motion parameters to constrain the laser calibration.

A. Constraining Motion Calibration with Laser Parameters

First, laser calibration is performed using the method from §II. Next, motion calibration is performed as follows. The same calibration board with the three checkerboard patterns from §III is placed parallel to the conveyor belt. The line lasers are also turned on. Images of the checkerboard patterns and the laser lines are captured together at various positions, along with either the encoder counts ΔE_i or the timestamp Δt_i.

Using the laser plane parameters alone, the detected laser points are triangulated, giving their 3D coordinates with respect to the camera center. Because two line lasers are present, the laser range data can be used to determine the plane $\boldsymbol{\pi}_c$ of the calibration board. The plane parameters $\boldsymbol{\pi}_c = (\hat{\boldsymbol{n}}_c, d_c)$ is recovered by finding the best-fit plane to all of the triangulated laser points (Eq. 3). To recover the translational direction $\hat{\boldsymbol{t}}$ of the conveyor belt, we form a constrained pose estimation problem similar to the one in §III, along with the additional constraint that all of the checkerboard poses $(\boldsymbol{R}_i, \vec{\boldsymbol{t}}_i)$ must lie on the calibration plane $\boldsymbol{\pi}_c$ defined by the laser points. To do so, we establish an arbitrary calibration pose $(\boldsymbol{R}_c, \vec{\boldsymbol{t}}_c)$ on the plane $\boldsymbol{\pi}_c$, and minimize the following cost function:

$$\underset{\psi,\vec{\boldsymbol{t}}_{c1},\theta,[v|\tau]}{argmin} \sum_j \left\| \boldsymbol{x_j} - \boldsymbol{K} \cdot \left[\boldsymbol{R}|\vec{\boldsymbol{t}}_i\right] \cdot \boldsymbol{X_j} \right\|^2 \quad (5)$$

Here, ψ is the angle of rotation of the checkerboard patterns from the calibration pose $\boldsymbol{R} = \boldsymbol{R_c} \cdot \boldsymbol{R_z}(\psi)$, and $\vec{\boldsymbol{t}}_{c1}$ is a 2D vector lying in the calibration plane $\boldsymbol{\pi}_c$ corresponding to the offset of the first checkerboard pose from the calibration pose, $\vec{\boldsymbol{t}}_1 = \vec{\boldsymbol{t}}_c + \boldsymbol{R_c} \cdot \left[\vec{\boldsymbol{t}}_{c1}{}^T, 0\right]^T$. Thus, the constrained problem has 4 to 5 DOF, corresponding to 3DOF for the first checkerboard pose, 1DOF for $\hat{\boldsymbol{t}}$, and 1 DOF for v or τ if desired.

B. Constraining Laser Calibration with Motion Parameters

First, motion calibration is performed using the method from §III. However, the laser lines are imaged together with the checkerboard patterns, and the process is repeated multiple times with the calibration board at different orientations $\boldsymbol{R^k}$ (Fig. 10).

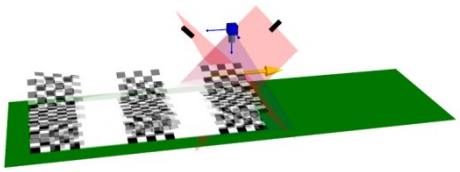

Figure 10. Constrained laser calibration.

Using the correspondences $\{\boldsymbol{X_j^k} \leftrightarrow \boldsymbol{x_j^k}\}$ between the checkerboard corners and their imaged coordinates, a single translational direction $\hat{\boldsymbol{t}}$ is estimated for the entire data set by minimizing the following cost function:

$$\underset{\boldsymbol{R^k},\vec{\boldsymbol{t}}_1^k,\theta,[v|\tau]}{argmin} \sum_j \left\| \boldsymbol{x_j^k} - \boldsymbol{K} \cdot \left[\boldsymbol{R^k}|\vec{\boldsymbol{t}}_i\right] \cdot \boldsymbol{X_j^k} \right\|^2 \quad (6)$$

Here, $(\boldsymbol{R^k}, \vec{\boldsymbol{t}}_1^k)$ is the initial pose of the calibration board for orientation $\boldsymbol{R^k}$. We assume that one of the orientations $\boldsymbol{R^p}$ is parallel to conveyor belt, so that the translational direction $\hat{\boldsymbol{t}}$ can still be parameterized using 1 DOF, $\hat{\boldsymbol{t}} = cos\theta\hat{\boldsymbol{\imath}} + sin\theta\hat{\boldsymbol{\jmath}}$, where $\hat{\boldsymbol{\imath}} = \boldsymbol{R^p} \cdot [1\ 0\ 0]^T$ and $\hat{\boldsymbol{\jmath}} = \boldsymbol{R^p} \cdot [0\ 1\ 0]^T$. For n_k different checkerboard orientations, the constrained problem has $6n_k + 1$ or $6n_k + 2$ DOF.

Using the checkerboard poses $(\boldsymbol{R^k}, \vec{\boldsymbol{t}}_i^k)$ and the laser points in the same images, laser calibration can be performed using the method from §II.

VI. Experiments and Validation

To validate the calibration methods presented above, a plane is placed at ten different positions and scanned, and the offset between the point clouds reconstructed from the two lasers is measured. As shown in Fig. 11, when laser calibration and motion calibration are performed independently, the misalignment error ranges between 0.5 to 5mm. When the motion calibration or the laser calibration is constrained by the other set of parameters, the error is dramatically reduced to 1.0mm and 0.4mm respectively.

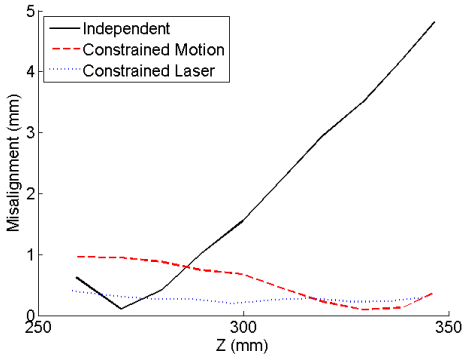

Figure 11. Misalignment errors between the point clouds of the two lasers of a plane scanned at 10 different position.

VII. Conclusions and Future Work

Our contribution in this paper is twofold. Firstly, as presented in §III, we have given a simple and economical solution to motion calibration – that is, the recovery of the direction of the translational motion – which has been neglected in most of the literature. This is especially important for a laser triangulation system in an assembly line environment, where the linear motion platform may not be well calibrated. Secondly, we addressed the issue of misalignment between point clouds when multiple lasers are used. We have given constrained solutions to the laser calibration and motion calibration problems to eliminate such misalignment. While laser and motion calibration are traditionally performed independent of one another, we have shown the significance of their interdependence in a multiple-lasers system.

Compared to the solution given by McIvor [10], which uses a single calibration object and procedure to simultaneously perform camera, laser, and motion calibration, we have given a modular solution, where each calibration is performed separately, with appropriate constraints. We believe that this is a more flexible approach, making it applicable to different types of setups. Also instead of using a single calibration object, from our experience, the three calibrations are best accomplished with different calibration objects – for camera calibration, the checkerboard pattern should cover a large part of the image, whereas for laser calibration, the checkerboard pattern should be smaller so that the laser line can cover different parts of the image, and for motion calibration, multiple checkerboard patterns is used to increase the range of motion. Furthermore, while McIvor's solution requires a 3D calibration object, our solution requires only the use of planar checkerboard patterns, which can be produced easily and inexpensively.

Future improvement includes minimizing the reprojection errors instead of the point-to-plane distances in the estimation of the laser plane parameters, and forming a combined calibration that simultaneously estimate both the laser and motion parameters.

References

[1] M. Munaro, S. Michieletto, E. So, and E. Menegatti, "Fast 2.5D model reconstruction of assembled parts with high occlusion for completeness inspection," International Conference on Machine Vision, Image Processing, and Pattern Analysis, 2011.

[2] E. So, M. Munaro, S. Michieletto, M. Antonello, and E. Menegatti, "Real-Time 3D Model Reconstruction with a Dual-Laser Triangulation System for Assembly Line Completeness Inspection," International Conference on Intelligent Autonomous Systems, 2012.

[3] C. Chen and A. Kak, "Modeling and calibration of a structured light scanner for 3-D robot vision," ICRA, 1987, vol. 4, pp. 807–815.

[4] I. D. Reid, "Projective calibration of a laser-stripe range finder," Image and Vision Computing, vol. 14, no. 9, pp. 659–666, 1996.

[5] D. Q. Huynh, R. A. Owens, and P. E. Hartmann, "Calibrating a structured light stripe system: a novel approach," IJCV, vol. 33, pp. 73–86, 1999.

[6] E. Trucco, R. B. Fisher, A. W. Fitzgibbon, and D. K. Naidu, "Calibration, data consistency and model acquisition with laser stripers," International Journal of Computer Integrated Manufacturing, vol. 11, no. 4, p. 293, 1998.

[7] F. Zhou and G. Zhang, "Complete calibration of a structured light stripe vision sensor through planar target of unknown orientations," Image and Vision Computing, vol. 23, no. 1, pp. 59–67, 2005.

[8] K. Yamauchi, Hideo Saito, and Y. Sato, "Calibration of a structured light system by observing planar object from unknown viewpoints," ICPR, 2008.

[9] Z. Zhang, "A flexible new technique for camera calibration," PAMI, vol. 22, no. 11, pp. 1330–1334, 2000.

[10] A. M. McIvor, "Nonlinear calibration of a laser stripe profiler," Optical Engineering, vol. 41, no. 1, p. 205, 2002.

[11] OpenCV Library, http://opencv.willowgarage.com/

[12] V.Vezhnevets, A.Velizhev, N.Chetverikov, A.Yakubenko, "GML C++ Camera Calibration Toolbox", http://graphics.cs.msu.ru/en/science/research/calibration/cpp, 2011.

[13] J.-Y. Bouguet, "Camera Calibration Toolbox for Matlab", http://www.vision.caltech.edu/bouguetj/calib_doc/, 2010.

[14] B. M. Haralick, C.-N. Lee, K. Ottenberg, and M. Nölle, "Review and analysis of solutions of the three point perspective pose estimation problem," IJCV, vol. 13, no. 3, pp. 331–356, 1994.

[15] D. K. Naidu and R. B. Fisher, "A comparative analysis of algorithms for determining the peak position of a stripe to sub-pixel accuracy," in BMVC, 1991, p. 217.

[16] S. J. Ahn, "Least Squares Orthogonal Distance Fitting of Curves and Surfaces in Space", Lecture Notes in Computer Science, vol. 3151, 2004.